# Influence of the B2-B19′ martnesitic transformation on the optical properties and electronic structure of intermetallic TiNi

I. I. Sasovskaya, S. A. Shabalovskaya, and A. I. Lotkov

*Institute of Metal Physics, Ural Scientific Center of the Academy of Sciences of the USSR, Sverdlovsk and V. D. Kuznetsov Siberian Physicotechnical Scientific-Research Institute at the State University, Tomsk*
(Submitted 14 April 1979)
Zh. Eksp. Teor. Fiz. 77, 2341–2349 (December 1979)

An investigation was made of the optical constants $n$ and $k$ of the equiatomic alloy TiNi in the photon energy range 0.07–4.9 eV; the measurements were carried out in the B2 and B19′ phases. Both phases were characterized by two groups of strong absorption bands in the visible and infrared parts of the spectrum. The martensitic transformation between these structures altered significantly only the infrared part of the spectrum, indicating a modification of the electron energy spectrum in the region of the Fermi level $E_F$. This modification was attributed to the formation, in the B19′ phase, of gaps resulting from the splitting of degenerate $d$ states. A possible origin of the instability of the B2 phase of TiNi was considered.

PACS numbers: 78.20.Dj, 71.25.Pi, 81.30.Kf

The intermetallic compound TiNi, characterized by the CsCl-type ordering, undergoes several martensitic transformations of the first and near-second order.[1-3] This variety of martensitic transformations occurring near room temperature is evidence of extreme instability of the CsCl structure in this system and suggests that the instability may be associated with the special features of the electron energy spectrum of TiNi near the Fermi level $E_F$. A theoreitcal calculation of the energy band spectrum of TiNi with the CsCl structure, carried out by the method of augmented plane waves (APW),[4] shows no singularities in the region of $E_F$.

Several experimental investigations of the electronic structure by x-ray spectroscopy have been reported.[5-8] Unfortunately, it is difficult to draw definite conclusions about the electronic structure of TiNi from these investigations because the structural state of the samples, which depend strongly on the composition and temperature, has not been monitored. This is why the existing data are frequency contradictory. For example, according to Ref. 9, the spectrum of nickel in TiNi has a sharp peak of the $d$ states near $E_F$, whereas there is no such structure according to Ref. 10.

The relationship between the electronic structure of TiNi and the martensitic transformations is discussed only in Refs. 11 and 12, where an analysis of the transport phenomena suggests a considerable shift of $E_F$ (~1.1 eV) as a result of this transformation and a change in the nature of the binding forces from predominantly covalent in the B2 phase to metallic in B19′. This analysis is made in the rigid-band model, postulating that the martensitic transformation does not alter the density of states $N(E)$ (Ref. 11). The conclusions reached in Refs. 11 and 12 are interesting but there are as yet no experimental results which would confirm them or conflict with them.

It follows that the currently available theoretical and experimental data on the electronic structure are clearly insufficient to establish how this structure changes as a result of martensitic transformations and what is its role in the realization of these transformations. This made it desirable to investigate the electronic structure of TiNi as a function of the crystal structure, composition, and temperature.

We investigated the optical properties of TiNi in two phases B2 and B19′, in the spectral range 0.07–4.9 eV ($\lambda = 17-0.26\mu$). This was one of the first attempts to detect the response of the optical characteristics to a martensitic transformation in an alloy. A similar investigation had been carried out earlier on alloys of the Fe–Ni system.[13] The present paper reports one of a series of experimental investigations of the electronic structure and its relationship to the crystal-structure transformations occurring in the compound TiNi near room temperature.

## PREPARATION OF THE SAMPLES

Equiatomic TiNi samples were produced by fusing electrolytic nickel and iodide titanium in an electric-arc furnace. The alloy composition was deduced from the weight of the ingot. Homogenization was ensured by sixfold fusion. Samples prepared for optical ($65 \times 10 \times 4$ mm) and x-ray structure investigations were annealed in vacuum of at least $10^{-5}$ Torr at 800 °C for 1 h (the melting point was 1300 °C) and then they were cooled together with the furnace; the purpose of this treatment was to remove the cold-working effects. Samples prepared in this way contained a second phase, whose amount (determined by the Rosewall method) amounted to 3–5% by volume. A specular optical surface was obtained by grinding with powders with various grain sizes, ending with M-5, and following this with electropolishing in an aged chloroacetic electrolyte (20% $HClO_4$ + 80% acetic anhydride by volume). The current density was 1 A/cm$^2$, the voltage was $V = 70$ volts, and the temperature was $T = 12-13$ °C. This electrolytic polishing removed a layer $50-30\mu$ thick. Optical surface-quality control[14] showed that this was sufficient to remove the cold-worked layer. The optical measurements were carried out on freshly prepared

 0038-5646/79/121128-05$02.40  

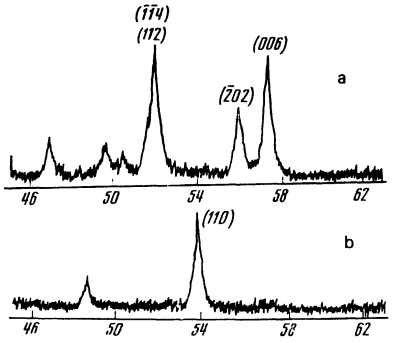


FIG. 1. X-ray diffractograms of equiatomic TiNi alloy obtained using unfiltered iron radiation (the unindexed lines correspond to $K_\beta$ radiation): a) martensitic (B19′ structure at $T = 20$ °C; b) austenitic (B2 structure at $T = 130$ °C.

surfaces (during the first 2–3 h after preparation). Before each series of measurements the samples were ground again with the M-7 and M-5 powders and electropolished anew.

The crystal structure and the characteristic transformation temperatures were determined by the x-ray structure method: the temperature was varied in steps of 5 °C (this was reduced to 2 °C in the vicinity of the martensitic transformation) and the profiles of the (110) and (220) lines were recorded for the B2 phase. An analysis of changes in the half-widths of the reflections showed that the B2–B19′ martensitic transformation occurred in our alloy without rhombohedral distortion of the original B2 structure. The transformation temperatures, deduced from the maximum intensities of the (110) and (220) reflections to within ±2 °C, were $M_s = 80$ °C and $M_f = 45$ °C (beginning and end of the transformation during cooling); $A_s = 100$ °C and $A_f = 120$ °C (beginning and end of the transformation during heating). We determined the optical properties of TiNi in the martensitic state at $T = 20$ °C (B19′) and in the austenitic state at $T = 130$ °C (B2). The x-ray diffractograms corresponding to these structural states are shown in Figs. 1a and 1b.

## EXPERIMENTAL METHOD

The optical constants $n$ and $k$ (refractive index and extinction coefficient) were determined by two modifications of the Beattie polarimetric method.[15] In the visible and ultraviolet parts of the spectrum (1–5 eV) use was made of a scheme with one reflection from the sample, which was studied with an SF-16 spectrometer and a GS-5 goniometer. The scheme used in the infrared range involved three reflections in which standard mirrors were substituted but only one sample was employed. Temperatures above the room value were obtained by pressing a heater to the rear side of a sample. In this case a thermocouple was attached to the specularly reflecting side of the sample.

The transformation to the austenitic phase by heating produced a fine relief on the specularly reflecting surface of a sample: the mirror-like surface finish was retained but its quality deteriorated. The spectrum obtained for such a surface at $T = 130$ °C was compared with that obtained for a specularly reflecting surface of a sample of the Ti–51 at.% Ni alloy kept at room temperature in the same structural state. In this alloy the martensitic transformation began at $T = 0$ °C during cooling. It was found that the surface relief simply reduced the optical absorption throughout the investigated wavelength range by four or five units of $\sigma$ ($\sigma$ is the optical frequency conductivity, Fig. 2b) and also reduced the real part of the permittivity $\varepsilon_1$. The observed change in $\sigma$ in the far infrared (a fall of $\sigma$ instead of a peak at 0.08 eV) was due to a difference in the composition and was not analyzed any further.

The rms error in the measurements of $n$ and $k$ was 2–3% in the visible range and 3–4% in the far infrared. The signal/noise ratio for the smallest of the measured components of the elliptically reflected polarized light ranged from 100:1 to 30:1 in the longest-wavelength part of the investigated range (10–17 $\mu$). Between five and seven independent series of measurements were carried out in each wavelength interval and the results were averaged and tabulated (Table I). The values of $n$ and $k$ obtained in this way were used to calculate the real $\varepsilon_1$ and imaginary $\varepsilon_2$ parts of the complex permittivity, optical-frequency conductivity $\sigma$, and other quantities derived from $n$ and $k$.

## INTERBAND ABSORPTION

We shall first consider the interband absorption results. Figure 2a shows the spectra of the optical-frequency conductivity $\sigma = nk\nu$ ($\nu$ is the frequency of light) for the austenitic and martensitic phases. It is clear from this figure both spectra have two strong absorption bands separated by a deep minimum. The energy position and the structure of the band in the visible part of the spectrum (1.2–4.9 eV) is not affected by the martensitic transformation. It is also clear from Fig. 2a that the edge of this absorption band is considerably steeper in the case of the austenitic phase. At the band edge there is a zero of $\varepsilon_1(\omega)$ and a maximum of the

TABLE I. Optical constants of intermetallic TiNi.

| λ, μ | Martensitic, T=20° C | | Austenitic, 130° C | | λ, μ | Martensitic, 20° C | | Austenitic, 130° C | |
|---|---|---|---|---|---|---|---|---|---|
| | n | k | n | k | | n | k | n | k |
| 0.2652 | 1.04 | 1.79 | — | — | 1.6 | 4.26 | 5.13 | 2.80 | 5.13 |
| 0.3022 | 1.13 | 2.13 | 1.24 | 2.06 | 1.8 | 4.57 | 5.37 | 2.96 | 5.74 |
| 0.3122 | 1.14 | 2.23 | 1.27 | 2.15 | 2.0 | 4.97 | 5.75 | 3.16 | 6.48 |
| 0.3340 | 1.18 | 2.37 | — | — | 2.05 | 4.70 | 6.00 | — | — |
| 0.3650 | 1.43 | 2.54 | 1.56 | 2.51 | 2.1 | 4.47 | 6.26 | — | — |
| 0.370 | 1.45 | 2.59 | 1.60 | 2.57 | 2.3 | 5.45 | 6.12 | 3.83 | 7.24 |
| 0.380 | 1.52 | 2.65 | 1.64 | 2.59 | 2.4 | 6.17 | 6.43 | 3.81 | 7.16 |
| 0.390 | 1.56 | 2.74 | 1.69 | 2.61 | 2.6 | 6.04 | 6.48 | 4.05 | 7.37 |
| 0.400 | 1.68 | 2.72 | 1.72 | 2.66 | 2.8 | 6.21 | 6.62 | 4.36 | 7.99 |
| 0.425 | 1.68 | 2.89 | 1.84 | 2.66 | 3.1 | 6.22 | 6.94 | 4.69 | 8.67 |
| 0.450 | 1.92 | 2.95 | 1.85 | 2.78 | 3.3 | 6.19 | 7.15 | 4.95 | 9.08 |
| 0.475 | 2.02 | 3.02 | 2.07 | 2.84 | 3.5 | 6.27 | 7.29 | 5.29 | 9.21 |
| 0.495 | — | — | 2.06 | 2.88 | 3.8 | 6.24 | 7.80 | 5.46 | 9.81 |
| 0.500 | 2.15 | 3.05 | 2.05 | 2.96 | 4.1 | 5.98 | 8.07 | 5.74 | 10.43 |
| 0.525 | 2.20 | 3.20 | 2.13 | 3.07 | 4.6 | 6.16 | 8.59 | 6.37 | 11.27 |
| 0.550 | 2.42 | 3.21 | 2.35 | 3.02 | 5.0 | 6.11 | 8.76 | 6.78 | 11.68 |
| 0.575 | 2.51 | 3.26 | 2.51 | 3.01 | 5.4 | 6.37 | 8.78 | 6.98 | 12.25 |
| 0.600 | 2.62 | 3.25 | 2.66 | 2.94 | 5.7 | 6.32 | 9.04 | 7.00 | 12.67 |
| 0.650 | 2.81 | 3.24 | 2.77 | 2.91 | 6.1 | 6.56 | 9.19 | 7.92 | 13.01 |
| 0.700 | 2.89 | 3.25 | 2.83 | 2.83 | 6.5 | 6.74 | 9.53 | 7.94 | 13.62 |
| 0.750 | 2.94 | 3.27 | 2.80 | 2.77 | 7.1 | 7.64 | 11.26 | 9.38 | 14.80 |
| 0.800 | 2.98 | 3.29 | 2.76 | 2.76 | 8.0 | 8.07 | 12.10 | 10.07 | 15.68 |
| 0.850 | 2.97 | 3.37 | 2.62 | 2.83 | 9.0 | 8.55 | 13.28 | 10.66 | 16.52 |
| 0.900 | 3.01 | 3.43 | 2.57 | 2.92 | 10.0 | 8.66 | 14.35 | 11.22 | 17.59 |
| 0.950 | 3.00 | 3.54 | 2.53 | 3.05 | 10.5 | — | — | 11.51 | 17.79 |
| 1.00 | 3.11 | 3.61 | 2.52 | 3.21 | 11.0 | 9.10 | 15.76 | 11.87 | 18.43 |
| 1.10 | 3.29 | 3.85 | 2.52 | 3.56 | 12.0 | 9.58 | 16.68 | 12.09 | 19.59 |
| 1.20 | 3.46 | 4.11 | 2.56 | 3.95 | 13.0 | 9.97 | 17.45 | 13.11 | 19.75 |
| 1.30 | 3.68 | 4.37 | 2.66 | 4.25 | 14.0 | 10.35 | 18.68 | 15.06 | 20.73 |
| 1.40 | 3.81 | 4.68 | 2.71 | 4.67 | 15.0 | 11.02 | 19.94 | 15.21 | 20.85 |
| 1.50 | 3.94 | 5.18 | 2.72 | 4.94 | 16.0 | 10.92 | 20.70 | 15.45 | 22.29 |
| | | | | | 17.0 | 11.65 | 21.14 | 15.68 | 22.46 |

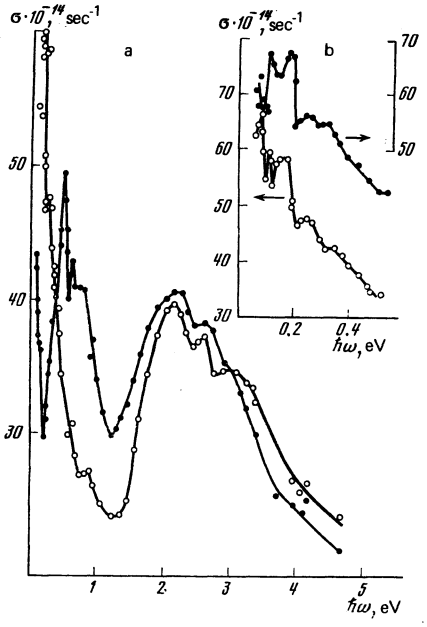


FIG. 2. Spectrum of optical-frequency conductivity $\sigma(\omega)$ of TiNi: a) austenitic phase (○) at 130°C and martensitic phase (●) at 20°C in alloy with 50 at.% Ni; b) infrared part of the spectrum of austenitic phase (○) in alloy with 50 at.% Ni at 130°C and of austenitic phase (●) in alloy with 51 at.% Ni at 20°C.

characteristic losses experienced by electrons $\varepsilon_2/(\varepsilon_1^2+\varepsilon_2^2)$ (Fig. 3), not observed for the martensitic phase. However, since the value of $\varepsilon_2$ is then quite high, an interband plasma resonance is hardly likely to occur.[16] The maximum at 3 eV transforms into an inflection in the case of martensite and the high-energy part of the band is narrowed by 0.2 eV.

The infrared part of the spectrum, where the second band is located, changes drastically as a result of the martensitic transformation. The conductivity $\sigma(\omega)$ of the austenitic phase rises continuously on reduction in the photon energy exhibiting interband absorption peaks right down to the lowest energies (0.085, 0.113, 0.17, 0.24, 0.35 eV), as shown in Fig. 2. In the case of the martensitic phase the onset of the interband absorption

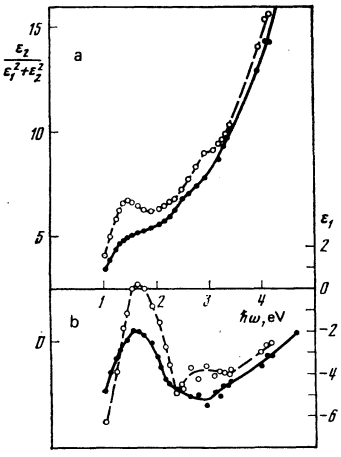


FIG. 3. Characteristic loss function of electrons (a) and dispersion of the real part of the permittivity (b) of austenitic (○) and martensitic (●) phases.

is shifted toward higher photon energies and, instead of all the austenite peaks, there is only a trace of a transition at 0.17 eV. However, the austenitic phase exhibits a new strong and complex band at 0.2–1.2 eV (6–1 μ) with maxima at energies of 0.52, 0.62, and 0.80 eV. The rise of $\sigma(\omega)$ in the range $\hbar\omega < 0.2$ eV is clearly due to the Drude-Zener contribution of free carriers.

## DISCUSSION OF INTERBAND ABSORPTION RESULTS

We shall consider the results obtained using the model of direct and also predominantly indirect transitions. The band structure of the B2 phase of TiNi was calculated by Papaconstantopoulos *et al.*,[4] who used the APW method. Unfortunately, they did not calculate the optical properties.

A large number of dipole-allowed direct transitions between parallel parts of the energy bands can be deduced from the absorption spectrum for several directions in the Brillouin zone, in addition to transitions between high-symmetry degenerate points in the zone. The energies of many of these transitions correspond to the spectral range ~1–4 eV, where a strong interband absorption band is located. These transitions occur between the energy bands 6 and 7–8 in the direction Δ at energies of 1.21 and 1.62 eV, respectively, between the energy bands 8–10 along $Z$ (1.62 eV), between the bands 4–8 (2.83 eV) and 6–7 (2.16 eV) in the direction $\Sigma$, and also between the bands 5–9 (2.56 eV) along $S$. One should note also a number of transitions between the high-symmetry points: $X_3$–$X_5$, (2.16 eV), $X_5$–$X_5$, (2.7 eV), and so on.

A comparison of these transitions with peaks in the experimental curve representing the optical-frequency conductivity of austenite (Fig. 2) accounts qualitatively for the position of the absorption band edge with the first maximum at 2.16 eV and a peak at 2.65 eV. In the energy band spectrum $E(k)$ given in Ref. 4 there are no direct transitions which might be responsible for the infrared interband absorption at $\hbar\omega < 0.35$ eV. We cannot exclude the possibility that such low-energy transitions can occur in internal parts of the Brillouin zone which are not reproduced in Ref. 4. The interband absorption in the visible part of the spectrum is described qualitatively by the model of direct transitions.

This analysis of the allowed direct transitions is based on the energy band spectrum of TiNi calculated for the $4s^2$ configuration and with the exchange factor 5/6 (Ref. 4). The energy band spectrum of TiNi obtained in the same investigation with the Slater exchange fails to account for the interband absorption in the visible and infrared parts of the spectrum.

In considering the optical-frequency conductivity on the basis of predominantly indirect transitions, we shall use the density-of-states curve $N(E)$ (Fig. 4b) obtained in Ref. 17 by calculating the energy band spectrum.[4] According to Ref. 17, $N(E)$ consists of two bands separated by a deep minimum at 1.2 eV below $E_F$. The calculation given there of the partial densities

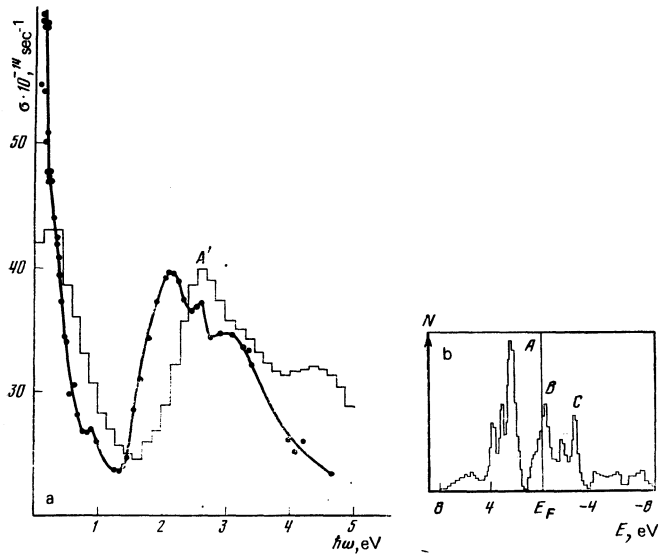


FIG. 4. a) Optical-frequency conductivity $\sigma(\omega)$ of the austenite phase of TiNi: the stepped curve represents calculations based on Eq. (1) and the points are experimental. b) Density-of-states curve $N(E)$ of the B2 structure of TiNi taken from Ref. 17.

of states shows that the structure of $N(E)$ in the filled part and above $E_F$ is determined by the $d$ states. The contribution of the $s$ and $p$ states is considerably less and it is negligible near $E_F$.

Using the complete density-of-states curve $N(E)$, we can calculate the interband optical-frequency conductivity $\sigma_{ib}(\omega)$ by applying the Berglund-Spicer formula and assuming that the elements of the transitions $W(E)$ are constant:

$$\sigma_{ib}(\omega) = \frac{W(E)}{\hbar\omega} \int_{E_F}^{E_F+\hbar\omega} N(E)\, N(E-\hbar\omega)\, dE.$$

We can see from Fig. 4a that the spectrum $\sigma_{ib}(\omega)$ has two absorption bands, like $\sigma_{exp}(\omega)$. The infrared band in $\sigma_{ib}(\omega)$ is due to electron transitions in the region of $E_F$ and carries information mainly on the $d$ states because, as mentioned above, these are the states that determine $N(E_F)$.

The structure of the $\sigma_{ib}(\omega)$ band is well resolved in the visible range and it repeats the features of $\sigma_{exp}(\omega)$. The maximum of $A'$ in $\sigma_{ib}(\omega)$ is due to transitions between the peaks $A$ (vicinity of the points $X_5$ and $\Gamma_{25'}$) and $B$ ($X_5$ and $\Gamma_{12}$) of $N(E)$, and also due to transitions from the Fermi surface to the peak $C$ (energy band 11 in $Z$ and $\Gamma$ directions). On the whole, the calculated optical-frequency conductivity $\sigma_{ib}(\omega)$ is in qualitatively good agreement with $\sigma_{exp}(\omega)$. However, the spectrum of $\sigma_{ib}(\omega)$ does not have a peak at 2.16 eV. This may be due to the fact that the peak in question is entirely due to the direct $X_3$–$X_5$, transitions or due to the fact that the $\sigma_{ib}(\omega)$ spectrum is shifted by 0.5 eV relative to $\sigma_{exp}(\omega)$. The former is not very likely because the general form of $\sigma_{ib}(\omega)$ reproduces well all the features of $\sigma_{exp}(\omega)$. A complete agreement between the positions of the $\sigma_{ib}(\omega)$ and $\sigma_{exp}(\omega)$ bands can be obtained if the $B$ and $C$ peaks of $N(E)$ are shifted by 0.5 eV closer to $E_F$.

The results of an experimental investigation of isochromes[7] support the hypothesis that the peak $C$ of $N(E)$ is indeed located closer to $E_F$ than predicted by the calculations. Lowering of the energy of the $d$ states ($\Gamma_{12}$, $X_{5'}$) has the effect that they coincide with the Fermi level. The shift of the peaks $B$ and $C$ corresponding to such lowering not only improves the agreement between $\sigma_{ib}(\omega)$ and $\sigma_{exp}(\omega)$ in the 1–5 eV range but also results in retention of the second absorption band in the lowest-energy part of $\sigma_{ib}(\omega)$ because the Fermi level then coincides with the density-of-states peak $B$.

The position of $E_F$ in the region of a narrow $N(E)$ peak [its width is equal to the step used in the calculations of $N(E)$ in Ref. 17] suggests an approach in the analysis of a possible reason for the instability of the B2 structure of TiNi: this approach is similar to that used in the case of compounds with the A15 crystal structure. In the majority of the models accounting for martensitic transformations in these compounds the necessary condition for the structural instability is a density-of-states peak near $E_F$ (Ref. 18). Such a position of $E_F$ in the case of TiNi ensures a likelihood of a structural transformation when temperature is lowered.

We shall now discuss the optical-frequency conductivity spectrum of TiNi in the B19′ state, shown in Fig. 2a. As mentioned earlier, the greatest changes as a result of the martensitic transformation are observed in the infrared range, indicating that the B2–B19′ phase transformation alters considerably the energy spectrum in the vicinity of $E_F$. Although this transformation changes the lattice structure from cubic to orthorhombic, there is little change in the deep states or in the states located above $E_F$ (peak $C$) and responsible for the absorption band located at ~1–5 eV in the Cs-Cl-type structure. The absence of significant changes in the position of the edge and maxima of the band in the visible part of the spectrum suggests that if $E_F$ does indeed shift as a result of the martensitic transformation, the shift cannot exceed 0.2 eV. This is confirmed by our investigation of the martensitic transformation in the alloy by photoelectron spectroscopy.

The disappearance of the long-wavelength infrared absorption band of martensite and the appearance of a strong asymmetric absorption peak at 0.52–0.80 eV indicate that gaps form along certain directions over a large part of the Brillouin zone in the region of $E_F$. These gaps are most likely due to lifting of the degeneracy of the states at the Fermi level ($\Gamma_{12}$, $X_{5'}$), so that some of the states drop below $E_F$ and some remain above the Fermi level. In the martensitic phase the density-of-states curve acquires a minimum near $E_F$.

The results obtained indicate that the change in the electronic structure as a result of the B2–B19′ martensitic transformation cannot be considered in the rigid-band model, as suggested by Mitchell *et al.*[11] However, the observed change in the nature of the electron energy spectrum in the region of $E_F$ suggests that the band energy changes may be an important factor in the B2–B19′ martensitic transformation. This is in agreement with the hypothesis of Mitchell *et al.* that this transformation in TiNi is of electronic origin.

## INTRABAND ABSORPTION

We shall now consider the intraband absorption results. An analysis of the dispersion of the real $\varepsilon_1 = n^2 - k^2$ and imaginary $\varepsilon_2 = 2nk$ parts of the complex permittivity in the wavelength range $17-7\mu$ shows that the situation is simplest in the martensitic phase.

In fact, the experimental dependence of $(1-\varepsilon_1)/\lambda^2$ on $\lambda^2$ is a straight line whose intercept gives the plasma frequency of the conduction electrons $\Omega^2 = 4.4 \times 10^{30}$ $\text{sec}^{-2}$. The experimental dependence $\sigma = \varphi(\varepsilon_1)$ gives $\gamma = 0.37 \times 10^{14}$ $\text{sec}^{-1}$.

The absence of frequency dispersion of $(1-\varepsilon_1)/\lambda^2$ shows that carriers in the martensitic phase are practically indistinguishable in respect of their relaxation frequency, forming a single hybridized conduction band. Consequently, in the case of the martensitic phase the dispersion of $\varepsilon_1$ and $\varepsilon_2$ can be described by simple Drude formulas.

The Drude-Zener formulas are completely inapplicable for the description of the dispersion of $\varepsilon_1$ and $\varepsilon_2$ of the austenitic phase of TiNi. The values of $\varepsilon_1$ and $\varepsilon_2$ for the austenitic phase behave typically like the majority of pure transition metals, exhibiting particularly a strong quadratic frequency dependence of the effective plasma $\Omega_{\text{eff}}^2 = (\varepsilon_1^2 + \varepsilon_2^2)\omega^2/\varepsilon_1$ and relaxation $\gamma = \varepsilon_2\omega/\varepsilon_1$ frequencies. This dependence may be due to two factors. One of them is the presence of several groups of carriers belonging to different sheets of the Fermi surface and characterized by very different relaxation frequencies; the other factor is a large contribution of the low-energy (and possibly zero-gap) intraband transitions. In the case under discussion, both factors are important.


[1]D. P. Dautovich and G. R. Purdy, Can. Metall. Q. **4**, 129 (1965).
[2]R. F. Hehemann, Metall. Trans. **2**, 39 (1971).
[3]D. B. Chernov, Yu. I. Paskal', V. É. Gyunter, A. A. Monasevich, and E. M. Savitskiĭ, Dokl. Akad. Nauk SSSR **247**, 854 (1979) [Sov. Phys. Dokl. **24**, 664 (1979)].
[4]D. A. Papaconstantopoulos and D. J. Nagel, Inst. J. Quantum Chem. Symp. No. 5, 515 (1971).
[5]V. V. Nemoshkalenko, Rentgenovskaya émissionnaya spektroskopiya metallov i splavov (X-Ray Emission Spectroscopy of Metals and Alloys), Naukova Dumka, Kiev, 1972, p. 158.
[6]E. Källne, J. Phys. **F4**, 167 (1974).
[7]H. Föll, Z. Phys. **B26**, 329 (1977).
[8]V. A. Trofimova, Kand. dissertatsiya (Thesis for Candidate's Degree), Sverdlovsk, 1978.
[9]J. R. Cuthill, A. J. McAlister, and M. L. Williams, J. Appl. Phys. **39**, 2205 (1968).
[10]A. S. Shulakov, T. M. Zimkina, V. A. Fomichev, and V. Ya. Nagornyĭ, Fiz. Tverd. Tela (Leningrad) **15**, 3598 (1973) [Sov. Phys. Solid State **15**, 2400 (1974)].
[11]M. A. Mitchell, F. E. Wang, and J. R. Cullen, J. Appl. Phys. **45**, 3337 (1974).
[12]N. G. Pace and G. A. Saunders, Philos. Mag. **22**, 73 (1970).
[13]I. I. Sasovskaya, M. M. Noskov, and A. Z. Men'shikov, Fiz. Met. Metalloved. **27**, 272 (1969).
[14]M. M. Kirillova, Zh. Eksp. Teor. Fiz. **61**, 336 (1971) [Sov. Phys. JETP **34**, 178 (1972)].
[15]J. R. Beattie, Philos. Mag. **46**, 235 (1955).
[16]J. P. Marton and B. D. Jordan, J. Appl. Phys. **49**, 4225 (1978).
[17]D. A. Papaconstantopoulos, J. W. McCaffrey, and D. J. Nagel, J. Phys. **F3**, L26 (1973).
[18]L. R. Testardi, M. Weger, and I. B. Goldberg, in: Superconducting Compounds with the $\beta$-Tungsten Structure (Russ. Transl.), Mir, M., 1977, p. 123.



Translated by A. Tybulewicz


# Optical properties of a semiconductor with an electron temperature superlattice


V. L. Bonch-Bruevich

*M. V. Lomonosov Moscow State University*



(Submitted 28 April 1979)
Zh. Eksp. Teor. Fiz. 77, 2351–2357 (December 1979)



The optical properties of a semiconductor in which an electron temperature superlattice has been produced are investigated. It is shown that under these conditions a crystal having a cubic lattice becomes, generally speaking, a biaxial crystal. The phase change on reflection of a normally incident wave is calculated for various experimental geometries. The shape of the superlattice is examined in an appendix. It is shown that within the limitations of the assumptions made in the calculations, the solutions represent "billows" such as are familiar in the Bénard hydrodynamical problem.



PACS numbers: 64.70.Kb, 61.50.Ks, 78.20.Bh


## 1. INTRODUCTION

A theory of the electron-temperature superlattice produced in a monopolar semiconductor when the electron gas is sufficiently heated by intraband absorption of electromagnetic radiation has been developed in Refs. 1–6. According to Refs. 2–6, this superlattice arises in the presence of band bending at the irradiated surface of the specimen when the intensity $I_m$ of the radiation at that surface exceeds a certain critical value $I_{cr}$. Then



0038-5646/79/121132-05$02.40